Journal of Crystal Growth ∎ (∎∎∎∎) ∎∎∎–∎∎∎

Contents lists available at ScienceDirect

Journal of Crystal Growth

journal homepage: www.elsevier.com/locate/jcrysgro

Phase composition, structure and properties of $(ZrO_2)_{1-x-y}(Sc_2O_3)_x(Y_2O_3)_y$ solid solution crystals ($x=0.08$–0.11; $y=0.01$–0.02) grown by directional crystallization of the melt

M.A. Borik [a], S.I. Bredikhin [b], V.T. Bublik [c], A.V. Kulebyakin [a], I.E. Kuritsyna [b], E.E. Lomonova [a], F.O. Milovich [c,*], V.A. Myzina [a], V.V. Osiko [a], P.A. Ryabochkina [d], S.V. Seryakov [c], N.Yu. Tabachkova [c]

[a] Prokhorov General Physics Institute, Russian Academy of Sciences, Vavilov Str. 38, 119991 Moscow, Russia
[b] Institute of Solid State Physics, Russian Academy of Sciences, Academician Osip'yan str. 2, Chernogolovka, Moscow District 142432, Russia
[c] National University of Science and Technology (MISIS), Leninskiy prospekt 4, 119049 Moscow, Russia
[d] Ogarev Mordovia State University, 68 Bolshevistskaya Str., Saransk 430005, Republic of Mordovia, Russia

ARTICLE INFO

Keywords:
A1. Solid solutions
A2. Skull melting, growth from high temperature melt
B1. ZrO_2–Sc_2O_3–Y_2O_3
B2. Ionic conducting materials
B3. Solid oxide fuel cells

ABSTRACT

For the first time crystals of the $(ZrO_2)_{1-x-y}(Sc_2O_3)_x(Y_2O_3)_y$ solid solutions ($x=0.08$–0.11; $y=0.01$–0.02) have been grown by directional melt crystallization. We have determined the range of melt compositions for which growth from the melt produces of the $(ZrO_2)_{1-x-y}(Sc_2O_3)_x(Y_2O_3)_y$ solid solution single crystals. The single-phase optically transparent single crystals following composition were grown: $(ZrO_2)_{0.9}(Sc_2O_3)_{0.08}(Y_2O_3)_{0.02}$; $(ZrO_2)_{0.89}(Sc_2O_3)_{0.09}(Y_2O_3)_{0.02}$; $(ZrO_2)_{0.89}(Sc_2O_3)_{0.10}(Y_2O_3)_{0.01}$; $(ZrO_2)_{0.88}(Sc_2O_3)_{0.10}(Y_2O_3)_{0.02}$. Comprehensive study of the crystal structure by using XRD, transmission electron microscopy, and Raman spectroscopy revealed that the all single crystals, which is identified by XRD data as cubic one, in fact have t″ tetragonal structure, which forms by small displacement of oxygen ions along the *c*-axis. Data on the phase stability of the crystals during mechanical crushing were obtained. The electrical conductivity was measured as a function of temperature by electrochemical impedance spectroscopy. It is established that $(ZrO_2)_{0.89}(Sc_2O_3)_{0.10}(Y_2O_3)_{0.01}$ crystals have the highest conductivity (0.168 S/cm at 1173 K).

1. Introduction

Scandia stabilized zirconia (ScZr) is a promising electrolyte for an application in solid oxide fuel cells (SOFC) that can operate at 1073–1123 K. The material exhibits the highest ionic conductivity among the zirconia solid solutions [1–4]. In practice, solid electrolytes are mainly used as gas-tight ceramic membranes fabricated by various ceramics technologies. The functional properties of these ceramic membranes largely depend on their microstructure (grain size, grain boundaries, intergranular stresses, porosity etc.) which are in turn controlled by the synthesis process conditions. Another method of obtaining zirconia materials is the synthesis of crystalline materials using melt crystallization methods, in particular, skull melting technique [5–8]. This approach facilitates the growth of high density monolithic crystalline material with zero porosity and no grain structure.

There are two main issues limiting practical use of the (ScZr): transformation of the high conductivity cubic phase into the rhombohedral phase at about 773–873 K [1], and high aging rate (conductivity degradation during extended exposure at operating temperatures) [9–11].

One method to improve the properties of the electrolyte materials, such as to stabilize the cubic modification, to suppress conductivity degradation is the introduction of second dopant (co-dopant) in addition to Sc^{3+} into the electrolyte structure. CeO_2 [12–14], Y_2O_3 [10,15], Yb_2O_3 [14–16], Gd_2O_3 [13,14,16], and Sm_2O_3 [14] were used as co-dopants.

Our previous investigation focused on crystal growth of $(ZrO_2)_{1-x}(Sc_2O_3)_x$ ($x=0.035$–0.11) solid solution by the directional crystallization of the melt [17]. In accord with the work it was found that the crystals contain the tetragonal+monoclinic ($x=0.035$), tetragonal ($x=0.06$; 0.09), and rhombohedral ($x=0.11$) phases. Therefore, in order to optimize the phase composition of ScZr crystals, yttria was introduced. Yttrium concentration was limited to 2 mol%, as it was shown in [10] that at higher yttria

* Corresponding author.
E-mail address: philippmilovich@gmail.com (F.O. Milovich).

http://dx.doi.org/10.1016/j.jcrysgro.2016.06.039
0022-0248/

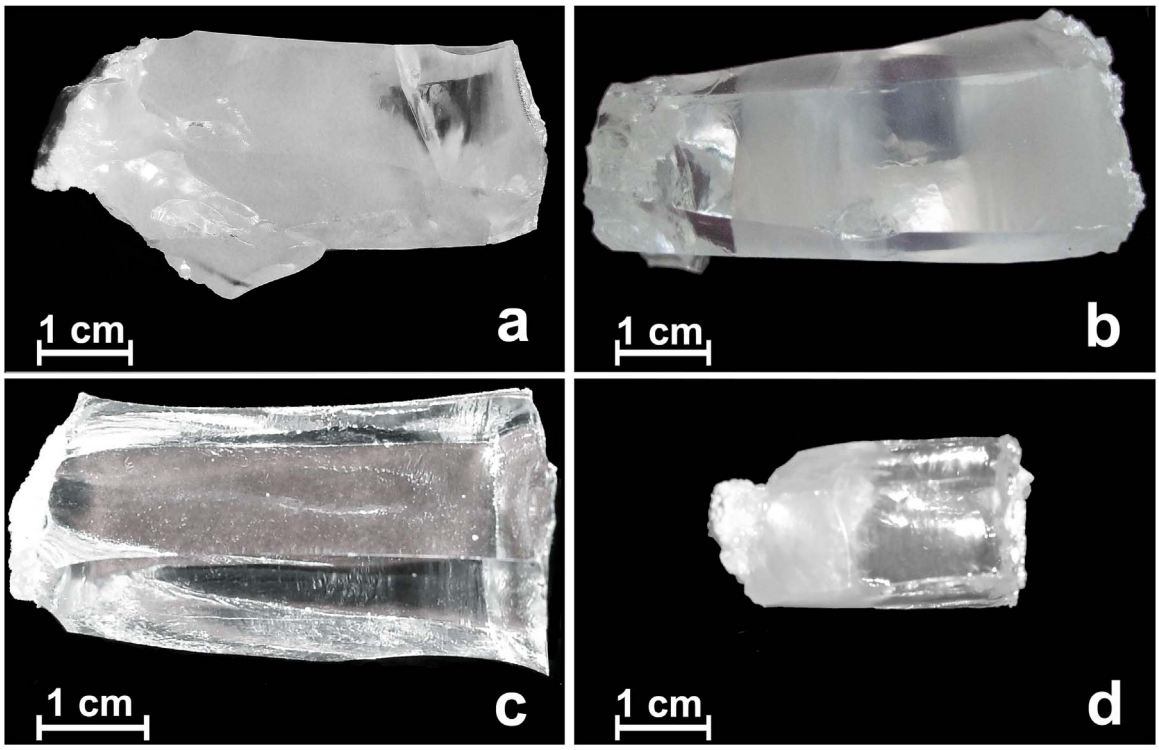

Fig. 1. Appearance of selected crystals: 8Sc1YZr (a); 9Sc1YZr (b); 8Sc2YZr (c) and 11Sc1YZr (d).

Table 1
The initial chemical compositions, descriptions and notations of the crystals.

Initial chemical composition	Notation	Description
$(ZrO_2)_{0.91}(Sc_2O_3)_{0.08}(Y_2O_3)_{0.01}$	8Sc1YZr	Semi-transparent (bottom) and transparent (top)
$(ZrO_2)_{0.90}(Sc_2O_3)_{0.09}(Y_2O_3)_{0.01}$	9Sc1YZr	Transparent and semi-transparent zones
$(ZrO_2)_{0.90}(Sc_2O_3)_{0.08}(Y_2O_3)_{0.02}$	8Sc2YZr	Fully transparent
$(ZrO_2)_{0.89}(Sc_2O_3)_{0.09}(Y_2O_3)_{0.02}$	9Sc2YZr	Fully transparent
$(ZrO_2)_{0.89}(Sc_2O_3)_{0.10}(Y_2O_3)_{0.01}$	10Sc1YZr	Fully transparent
$(ZrO_2)_{0.88}(Sc_2O_3)_{0.1}(Y_2O_3)_{0.02}$	10Sc2YZr	Fully transparent
$(ZrO_2)_{0.88}(Sc_2O_3)_{0.11}(Y_2O_3)_{0.01}$	11Sc1YZr	Semi-transparent (bottom) and transparent (top)

concentrations decreased electrical conductivity occurred. Objective of the present investigation is to study the crystal growth and the effect of yttria co-doping on the phase composition, structure and properties of $(ZrO_2)_{1-x-y}(Sc_2O_3)_x(Y_2O_3)_y$ solid solution crystals ($x=0.08-0.11$; $y=0.01-0.02$).

2. Experimental procedure

$(ZrO_2)_{1-x-y}(Sc_2O_3)_x(Y_2O_3)_y$ solid solution single crystals were grown by directional crystallization of the melt in a water-cooled copper crucible 130 mm in diameter. The growth installation was Kristall-407 (frequency 5.28 MHz, maximum output power 60 kW). The charge weight was 6 kg. ZrO_2, Sc_2O_3 and Y_2O_3 powders of not less than 99.99% purity grade were the initial materials. The directional crystallization of the melt was performed by moving the crucible with the melt downward relative to the induction coil at a 10 mm/h rate. The as-grown ingots consisted of a large number of column crystals that could be mechanically separated into individual crystals. The weight of the ingots was 4.5–5.0 kg. After the installation was shut down the ingot cooled down spontaneously. The cooling of the ingots was monitored by measuring the temperature on the surface of the upper heat screen with a Gulton 900–1999 radiation pyrometer (above 1273 K) and a Pt/Pt-Rh thermocouple (1273 K down to 773 K). The

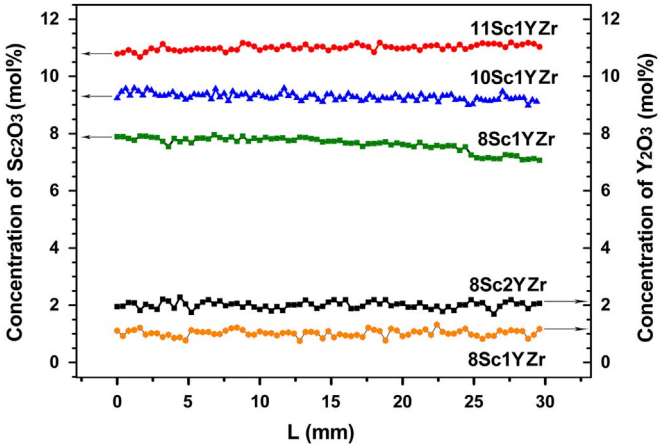

Fig. 2. Scandia and yttria distribution along the 11Sc1YZr, 10Sc1YZr, 8Sc1YZr, 8Sc2YZr crystals.

Table 2
Scandia and yttria distribution in the turbid and transparent parts of the crystals.

Specimen		Composition (mol%)[a]		
		Sc_2O_3	Y_2O_3	ZrO_2
8Sc1YZr	Transparent part	7.16 ± 0.07	1.01 ± 0.08	91.83 ± 0.10
	Turbid part	7.63 ± 0.05	0.97 ± 0.07	91.40 ± 0.09
11Sc1YZr	Transparent part	10.58 ± 0.04	1.06 ± 0.08	88.37 ± 0.09
	Turbid part	10.71 ± 0.04	0.97 ± 0.06	88.32 ± 0.06
9Sc1YZr	Transparent part	8.86 ± 0.04	1.074 ± 0.05	90.05 ± 0.06
	Turbid part	8.23 ± 0.06	0.82 ± 0.06	90.86 ± 0.12

[a] The average concentrations from the measurements at five points.

Table 3
Phase composition, crystal structure parameters, density and microhardness of $(ZrO_2)_{1-x-y}(Sc_2O_3)_x(Y_2O_3)_y$ solid solution crystals.

Specimen		Phase	Space group	Lattice parameters, Å	Density (g/cm^3)	Microhardness HV (kg/mm^2)	Load (g)
8Sc1YZr	Turbid part	t-ZrO_2	$P4_2/nmc$	$a=3.6002(5)$ $c=5.1192(5)$	5824(1)	1425 ± 40	50
	Transparent part	c-ZrO_2	$Fm\bar{3}m$	$a=5.1033(5)$		1450 ± 40	50
8Sc2YZr	Transparent crystal	c-ZrO_2	$Fm\bar{3}m$	$a=5.1012(5)$	5811(1)	1530 ± 50	25
9Sc1YZr	Turbid part	t-ZrO_2	$P4_2/nmc$	$a=3.6009(5)$ $c=5.1090(5)$	5769(5)	1510 ± 40	50
		c-ZrO_2	$Fm\bar{3}m$	$a=5.0947(5)$			
	Transparent part	c-ZrO_2	$Fm\bar{3}m$	$a=5.0954(5)$		1530 ± 40	100
9Sc2YZr	Transparent crystal	c-ZrO_2	$Fm\bar{3}m$	$a=5.0982(5)$	5760(1)	1505 ± 40	50
10Sc1YZr	Transparent crystal	c-ZrO_2	$Fm\bar{3}m$	$a=5.0932(5)$	5.744(1)	1550 ± 40	50
10Sc2YZr	Transparent crystal	c-ZrO_2	$Fm\bar{3}m$	$a=5.0961(5)$	5741(2)	1470 ± 25	100
11Sc1YZr	Turbid part	r-ZrO_2	$R\bar{3}m$	$a=3.561(1)$ $c=9.022(2)$	5720(2)	1530 ± 40	50
		c-ZrO_2	$Fm\bar{3}m$	$a=5.087(1)$			
	Transparent part	c-ZrO_2	$Fm\bar{3}m$	$a=5.0912(5)$		1684 ± 45	100

t-tetragonal, c-cubic, r-rhombohedral. The digits stated in brackets represent the standard deviation of the determined values with respect to the last significant digit.

average ingot cooling rate from the melt temperature to 1273 K was 150–200 K/min and then down to 773 K, 30 K/min. Typical dimensions of the crystals were 10–18 mm in cross-section and 30–50 mm in length.

The chemical composition of the crystals was determined by X-ray spectral analysis under a JEOL 5910 LV (Japan) electron scanning microscope equipped with INCA ENERGY (Oxford Instruments, England) energy dispersive (EDS) system. Melted zirconia, yttria and scandia were used as standards. The accuracy in determining the concentration of these elements was $\pm 5\%$ of the measured value.

Phase analysis was carried out using Raman scattering spectroscopy on a Renishawin Via Raman spectrometer and X-ray diffraction (XRD) on a Bruker D8 diffractometer in CuKα-radiation with a position sensitive LYNXEYE detector, the DIFFRAC software package and PDF-2 data bank. The measurements of the lattice parameters was carried out using X-ray parallel beam method on the plates that were cut from the crystal perpendicular to the $<100>$ direction. Selected area electron diffraction (SAED) patterns and TEM images were obtained using transmission electron microscope JEM 2100 at an acceleration voltage of 200 keV. For electron microscopic studied we cut wafers perpendicular to the $<111>$ direction. SAED patterns were taken from specimen area with the diameter of about 1 μm.

The density of the crystals was measured by hydrostatic weighing on a Sartorius balance (measuring error 0.05%). The microhardness of the crystals was measured on a DM 8 B AUTO microhardness tester with a 25–100 g load.

The ionic conductivity of the crystals was studied in the 623–1173 K range with 50 K steps using a Solartron SI 1260 frequency analyzer at 1–5 MHz range and 24 mV ac amplitude signal. The measurements were carried out on crystal plates with sizes of 7*7 mm^2 and thickness of 0.5 mm with symmetrically connected platinum electrodes. Platinum electrodes were burned in air at a temperature of 1223 K. The resistivity was measured in a measurement cell using the four-probe method in a Nabertherm high temperature furnace (Nabertherm GmbH, Germany). The impedance frequency spectrum was analyzed in detail using the ZView (ver. 2.8) (Scribner Associates, Inc., USA) software. The resistivity of the crystals was calculated based on the resultant impedance spectra, and then the specific conductivities of the crystals were calculated. Equivalent circuits described earlier were used for the calculation of the impedance spectra [18].

3. Results and discussion

The single crystals of the $(ZrO_2)_{1-x-y}(Sc_2O_3)_x(Y_2O_3)_y$ solid solution ($x=0.08$–0.11; $y=0.01$–0.02) were grown by the skull melting technique. The as-grown single crystals had the columnar shapes typical for this growth technique. Dimensions of the crystals were 10–18 mm in cross-section and 30–50 mm in length (Fig. 1).

Obtained crystals were free of micro and macro cracks, unlike the $(ZrO_2)_{1-x}(Sc_2O_3)_x$ solid solution crystals [17]. The 8Sc2YZr, 9Sc2YZr, 10Sc1YZr and 10Sc2YZr crystals were optically homogeneous and transparent without any visible defects. The 8Sc1YZ, 9Sc1YZr, and 11Sc1YZr crystals were optically inhomogeneous and had a transparent and semi-transparent zones located perpendicular to the growth direction.

The initial chemical compositions, descriptions and notations of the crystals are presented in Table 1.

Scandia and yttria tipical distribution along the 8Sc1YZr, 8Sc2YZr, 10Sc1YZr, 11Sc1YZr crystals is shown in Fig. 2. (The figure shows not all curves for the sake of clarity).

Scandia and yttria distribution along 11Sc1YZr, 10Sc1YZr, 8Sc2YZr crystals is homogeneous. This indicates that the effective distribution coefficient of Sc and Y is close to 1. Scandia distribution along 8Sc1YZr crystal indicates decreasing of scandia concentration in top (transparent) part of the crystal. This is in agreement with results of chemical composition measurement of transparent and turbid parts of 8Sc1YZr, 9Sc1YZr and 11Sc1YZr (Table 2). These measurements showed that the transparent parts of the crystals contain slightly more yttria and less scandia compared to the turbid parts.

The XRD study showed that uniform, transparent crystals 8Sc2YZr, 9Sc2YZr, 10Sc1YZr and 10Sc2YZr are single phase with cubic fluorite structure. The unit cell parameter of the cubic solid solutions decreases with increasing Sc_2O_3 concentration at a constant concentration of Y_2O_3. Data on the phase composition, crystal structure, density and microhardness of the obtained crystals are given in Table 3.

The phase composition of the optical inhomogeneous crystals was measured separately on samples cut from transparent and turbid parts of the crystal. The transparent parts of the 8Sc1YZr, 9Sc1YZr and 11Sc1YZr crystals, according to XRD, had a cubic structure. The turbid part of the 8Sc1YZr crystals was single phase and tetragonal with tetragonality $c/\sqrt{2}a=1.005$. The turbid part of the 9Sc1YZr crystals contains two phases, the cubic and the tetragonal one with tetragonality $c/\sqrt{2}a=1.003$. The turbid part of

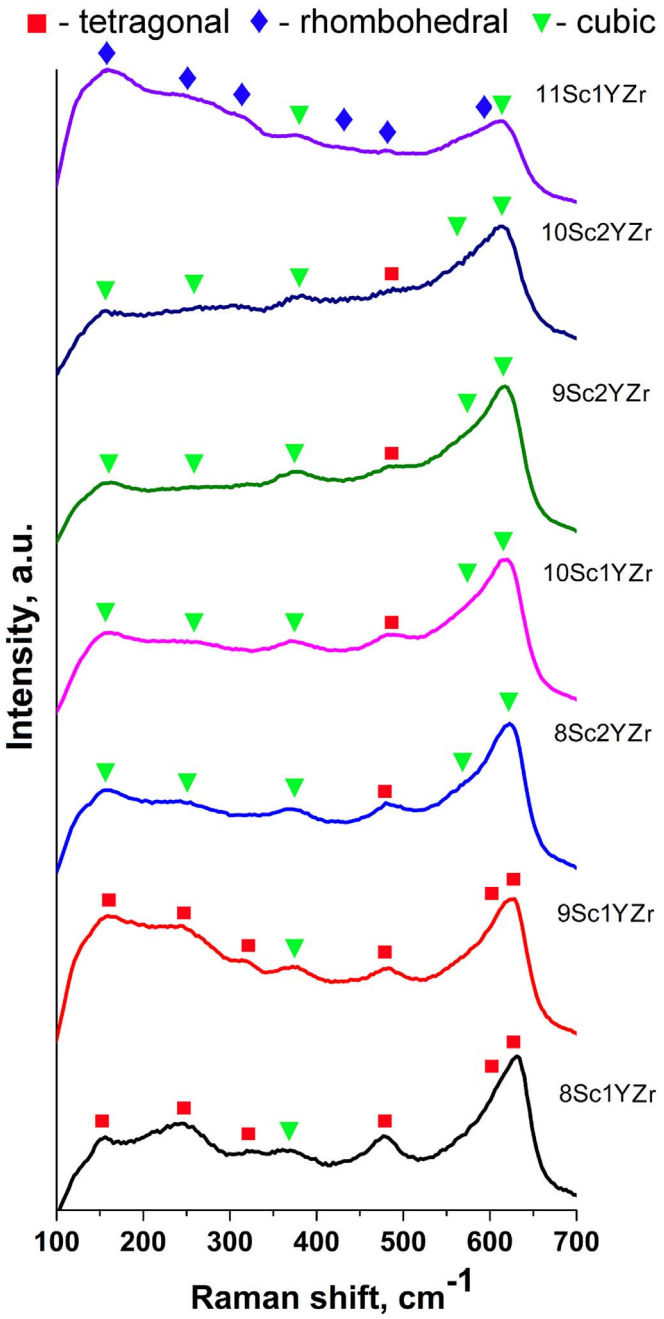

Fig. 3. Raman spectra of the $(ZrO_2)_{1-x-y}(Sc_2O_3)_x(Y_2O_3)_y$ solid solution crystals. (Identification of the peaks corresponding to the tetragonal, cubic, and rhombohedral phases in accordance with [19–21]).

the 11Sc1YZr crystals was a mixture of rhombohedral and cubic phases.

The data presented in Fig. 1 and Tables 2 and 3 show that even minor local fluctuations in the composition of the crystals with 1 mol% Y_2O_3 can lead to the nucleation and growth of second phases during the growth and cooling of crystals. Probably, co-doping of ScZr by 1 mol% Y_2O_3 is insufficient for the growth of cubic single phase solid solution crystals.

The density of the crystals depended on the type and concentration of stabilizing oxides, and the phase composition of the crystals. The highest density had the crystals containing a tetragonal phase. For example, the densities of the 8Sc1YZr and 9Sc1YZr crystals containing also the tetragonal phase are higher than the density of the 8Sc2YZr and 9Sc2YZr cubic crystals. The density of the 8Sc2YZr, 9Sc2YZr, 10Sc1YZr, and 10Sc2YZr homogeneous cubic crystals decreases with increasing total concentration of stabilizing oxides. When equal the total concentration of stabilizing oxide, the density of the crystals decreased with increasing concentration of Sc_2O_3, since the mass to volume ratio for Sc^{3+} ion is less than for the Y^{3+} ion. The 11Sc1YZr crystals had minimal density, due to the presence of inclusions of rhombohedral phase in volume of the crystal.

The crystals have high microhardness and low fracture toughness. Table 3 shows the limit indenter loads to specimen cracking and the microhardness measured at these loads.

The phase composition of the powders, obtained by crushing and grinding the crystals, was investigated by using XRD in order to assess their phase stability to mechanical impact. The powders of inhomogeneous crystals were prepared separately from the transparent and turbid parts of crystals. A change in the phase composition of the four homogeneous fully transparent 8Sc2YZr, 9Sc2YZr, 10Sc1YZr and 10Sc2YZr cubic crystals after mechanical crushing of the specimens was only observed in the 10Sc2YZr specimen. The cubic to rhombohedral transformation was observed after grinding of 10Sc2YZr crystals. The mechanical crushing of 8Sc2YZr, 9Sc2YZr and 10Sc1YZr crystals did not lead to a change in the phase composition and the powders retained the original cubic structure of the crystals.

A qualitative change in the phase composition in turbid parts of all inhomogeneous powdered crystals was not observed, but transparent parts of all inhomogeneous powdered crystals were not resistant to mechanical impact. A partial cubic to tetragonal phase transition was observed in transparent parts of the 8Sc1YZr, 9Sc1YZr powdered crystals. The cubic to rhombohedral phase transition was observed in the transparent part of the 11Sc1YZr powdered sample. Thus, it can be assumed that the chemical composition of the cubic phase in the transparent areas of inhomogeneous crystals is close to the two-phase boundary in the respective phase diagram.

The phase compositions of the crystals were studied by using Raman spectroscopy. Raman spectra of the $(ZrO_2)_{1-x-y}(Sc_2O_3)_x(Y_2O_3)_y$ as-grown crystals are shown in Fig. 3.

The Raman spectra of the 11Sc1YZr crystals contain peaks corresponding to the cubic and rhombohedral phases. The spectra of the 8Sc1YZr and 9Sc1YZr crystals have peaks of the tetragonal and cubic phases.

The spectra of cubic crystals 8Sc2YZr, 9Sc2YZr, 10Sc1YZr, 10Sc2YZr similar to each other and contain peaks corresponding to cubic phase [19–21]. The spectra of these crystals also contain a peak located at 483 – 487 cm^{-1}, which the authors of a number of studies [21–23] attributed to the t″ - phase. The t″ - phase is characterized by the axial ratio $c/\sqrt{2}a=1$ and a small displacement of oxygen ions along the *c*-axis, which leads to a tetragonal symmetry (space group of $P4_2/nmc$). The t″ - phase is observed in arc-melted ZrO_2–Y_2O_3 samples [21], thermal barrier coatings [24] and films of solid electrolytes [25]. The peak located at about 470 cm^{-1} is also observed in the Raman spectra of the ZrO_2–8 mol% Y_2O_3 crystals, obtained by directional crystallization of the melt [26]. This peak is absent in the Raman spectra of crystals with concentrations ranging 12–20 mol% Y_2O_3 [26]. It should be noted that the composition ZrO_2–8 mol% Y_2O_3, which is a boundary between t″ and the cubic structure, shows a maximum ionic conductivity in the system ZrO_2–Y_2O_3. Raman spectroscopy allows to distinguish the t″ - phase from the cubic one, as it is more sensitive to distortions in the anionic sub-lattice.

The study of the turbid parts of the crystals 8Sc1YZr and 8Sc2YZr (which have different space groups by XRD data) was carried out by transmission electron microscopy to determine the details of the fine crystal structure. Fig. 4 shows the TEM images and electron diffraction patterns of the 8Sc1YZr and 8Sc2YZr

Please cite this article as: M.A. Borik, et al., Journal of Crystal Growth (2016), http://dx.doi.org/10.1016/j.jcrysgro.2016.06.039

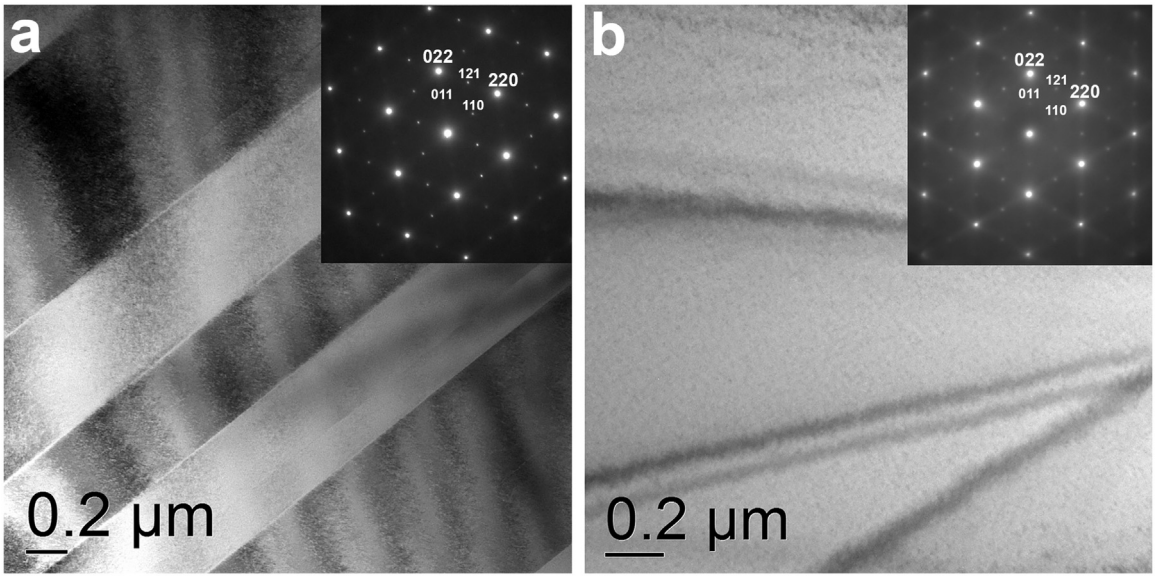

Fig. 4. TEM images of the 8Sc1YZr (turbid part) (a) and 8Sc2YZr (b) crystals. The insets show electron diffraction patterns of the respective crystal specimen regions.

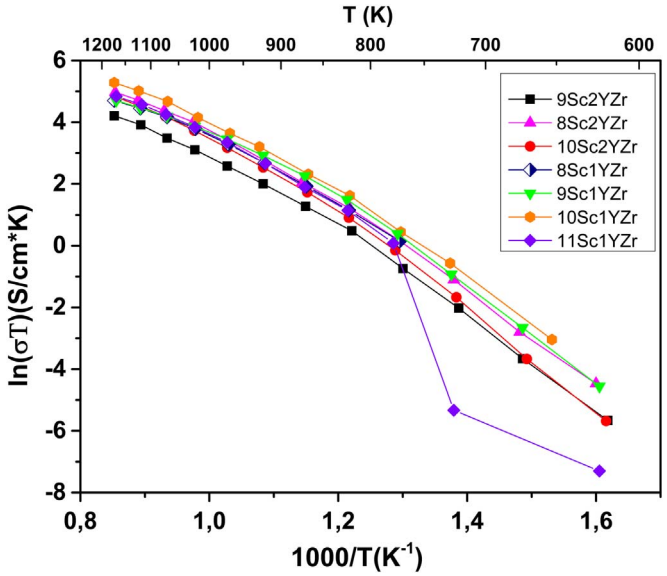

Fig. 5. Arrhenius plot of electrical conductivities for the $(ZrO_2)_{1-x-y}(Sc_2O_3)_x(Y_2O_3)_y$ solid solutions crystals.

Table 4
Conductivities of the $(ZrO_2)_{1-x-y}(Sc_2O_3)_x(Y_2O_3)_y$ solid solution crystals in the 973–1173 K range.

Material	Conductivity (mS/cm)			
	973 K	1073 K	1123 K	1173 K
8Sc1YZr	28	62	77	93
9Sc1YZr	31	63	78	94
8Sc2YZr	32	80	101	133
9Sc2YZr	13	30	46	55
10Sc1YZr	40	100	126	168
10Sc2YZr	24	63	84	116
11Sc1YZr	29	66	88	108

samples.

The morphologies of the 8Sc1YZr and 8Sc2YZr samples are different. Fig. 4 shows that 8Sc1YZ tetragonal crystal with tetragonality $c/\sqrt{2}a = 1.005$ contains twins. There are no twins present within the 8Sc2YZr samples. This TEM image is typical for the nearly defect-free cubic single crystals. Importantly, the diffraction pattern of the 8Sc2YZr sample shows reflections forbidden for a cubic lattice and permitted for the tetragonal structure ($P4_2/nmc$). The presence of such reflections like 110 and 121 indicate to an ordered displacement of oxygen atoms from ideal positions and breaking of the $Fm\bar{3}m$ space symmetry.

Therefore, comprehensive study of the crystal structure by using XRD, transmission electron microscopy, and Raman spectroscopy revealed that the 8Sc2YZr, which is identified by XRD data as cubic one, in fact has t″ tetragonal structure. Apparently, this conclusion is also valid for single-phase cubic (by XRD) 9Sc2YZr, 10Sc1YZr, 10Sc2YZ crystals as detected by Raman spectroscopy.

The specific ionic conductivity (σ) of the crystal samples was calculated based on the analysis of the impedance spectra recorded at a constant temperature taking into account the sizes of the samples using the following formula:

$$\sigma = (1/R)(l/S) \quad (1)$$

where R is the sample resistance, l is the specimen thickness and S is the contact area.

The dependences of conductivity on the inverse temperature in the Arrhenius coordinates are shown in Fig. 5.

A large step in the conductivity curve is observed in the 11Sc1YZr crystals at 723–773 K. This is indicative of the rhombohedral to cubic phase transition and consistent with our data on the phase composition of the crystal (Table 3) and published data [1,10,14].

Data on conductivities of the $(ZrO_2)_{1-x-y}(Sc_2O_3)_x(Y_2O_3)_y$ solid solution crystals are presented in Table 4.

Comparing the conductivity of $(ZrO_2)_{1-x-y}(Sc_2O_3)_x(Y_2O_3)_y$ single-phase crystals one can note that the 10Sc1YZr sample has the highest ionic conductivity and the conductivity of 9Sc2YZr samples was minimum in the whole temperature range. This is not consistent with previous results on the study $(Y_2O_3)_x(Sc_2O_3)_{(11-x)}(ZrO_2)_{89}$ ceramics [10] according to which the maximum conductivity was observed for the Y2Sc9Zr89 sample. A probable origin of this discrepancy is that our experimental crystals were grown from the melt, and therefore their thermal history differs significantly from that of the ceramic specimens. For example, in [15] it has been shown that different heat treatment can

significantly affect the conductivity of ceramic materials of the same chemical composition. The 8Sc1YZr, 9Sc1YZr and 11Sc1YZr inhomogeneous crystals have almost the same conductivity.

4. Summary

For the first time crystals of the $(ZrO_2)_{1-x-y}(Sc_2O_3)_x(Y_2O_3)_y$ solid solutions ($x=0.08–0.11$; $y=0.01–0.02$) have been grown by directional melt crystallization. It was found that additional doping of the crystals, containing 8 or 9 mol% Sc_2O_3, with 1 mol% Y_2O_3 is insufficient to obtain single-phase and optically transparent crystals. Increasing Y_2O_3 content to 2 mol% (8Sc2YZr and 9Sc2YZr compositions) leads to the formation of single crystals with a cubic fluorite-type crystal structure as determined by XRD which was also retained after mechanical crushing. The crystal 10Sc2YZr, unlike 10Sc1YZr, undergo the cubic to rhombohedral transformation after grinding, but the both crystals were also single-phase and optically transparent. This indicated a low phase stability of the 10Sc2YZr crystals. Thus, the overall concentration of the stabilizing oxides ≥ 12 mol% can cause the formation of the rhombohedral phase. Comprehensive study of the crystal structure by using XRD, transmission electron microscopy, and Raman spectroscopy revealed that the 8Sc2YZr, 9Sc2YZr, 10Sc1YZr, and 10Sc2YZr crystals, which is identified by XRD data as cubic one, in fact have t″ tetragonal structure, which forms by small displacement of oxygen ions along the *c*-axis. Thus, we have determined the range of melt compositions for which growth from the melt produces $(ZrO_2)_{1-x-y}(Sc_2O_3)_x(Y_2O_3)_y$ solid solution single crystals ($x=0.08–0.11$; $y=0.01–0.02$). The ionic conductivity study of the obtained crystals shows that the 10Sc1YZr crystals have the highest conductivity (0.168 S/cm at 1173 K).

Acknowledgments

This work was carried out within ofi_m No. 14-29-04081 RFBR Project and with the support from the Ministry of Education and Science of the Russian Federation, Project No. 16.1733.2014/K.

References

[1] S.P.S. Badwal, F.T. Ciacchi, D. Milosevic, Scandia-zirconia electrolytes for intermediate temperature solid oxide fuel cell operation, Solid State Ion. 136–137 (2000) 91–99.
[2] V.V. Kharton, F.M.B. Marques, A. Atkinson, Transport properties of solid oxide electrolyte ceramics: a brief review, Solid State Ion. 174 (2004) 35–49.
[3] J.W. Fergus, Electrolytes for solid oxide fuel cells, J. Power Sources 162 (2006) 30–40.
[4] H. Yokokawa, N. Sakai, T. Horita, K. Yamaji, M.E. Brito, Solid oxide electrolytes for high temperature fuel cells, Electrochemistry 73 (2005) 20–30.
[5] M.A. Borik, M.A. Vishnyakova, V.P. Voitsitskii, A.V. Kulebyakin, E.E. Lomonova, V.A. Myzina, V.V. Osiko, V.A. Panov, Preparation and properties of Y_2O_3 partially stabilized ZrO_2 crystals, Inorg. Mater. 43 (2007) 1223–1229.
[6] V.V. Osiko, M.A. Borik, E.E. Lomonova, Synthesis of refractory materials by skull melting, in: G. Dhanaraj, K. Byrappa, V. Prasad, M. Dudley (Eds.), Springer handbook of crystal growth, Springer, New York, 2010, pp. 433–477.
[7] M.A. Borik, E.E. Lomonova, V.V. Osiko, V.A. Panov, O.E. Porodinkov, M. A. Vishnyakova, Yu.K. Voron'ko, V.V. Voronov, Partially stabilized zirconia single crystals: growth from the melt and investigation of the properties, J. Cryst. Growth 275 (2005) e2173–e2179.
[8] S. Berendts, M. Lerch, Growth of yttria-doped zirconium oxide nitride single crystals by means of reactive skull melting, J. Cryst. Growth 336 (2011) 106–111.
[9] S.P.S. Badwal, F.T. Ciacchi, S. Rajendran, J. Drennan, Solid State Ion. 109 (1998) 167–186.
[10] T.I. Politova, J.T.S. Irvine, Investigation of scandia–yttria–zirconia system as an electrolyte material for intermediate temperature fuel cells – influence of yttria content in system $(Y_2O_3)_x(Sc_2O_3)_{(11-x)}(ZrO_2)_{89}$, Solid State Ion. 168 (2004) 153–165.
[11] K. Du, C.-H. Kim, A.H. Heuer, R. Goettler, Z. Liu, Structural evolution and electrical properties of Sc2O3)-stabilized ZrO2 aged at 850 °C in air and wet-forming gas ambients, J. Am. Ceram. Soc. 91 (2008) 1626–1633.
[12] D.S. Lee, W.S. Kim, S.H. Choi, J. Kim, H.-W. Lee, J.H. Lee, Characterization of ZrO_2 Co- doped with Sc_2O_3 and CeO_2 electrolyte for the application of intermediate temperature SOFCs, Solid State Ion. 176 (2005) 33–39.
[13] H.A. Abbas, C. Argirusis, M. Kilo, H.D. Wiemhöfer, F.F. Hammad, Z.M. Hanafi, Preparation and conductivity of ternary scandia-stabilised zirconia, Solid State Ion. 184 (2011) 6–9.
[14] S. Omar, W.B. Najib, W. Chen, N. Bonanos, Electrical conductivity of 10 mol% Sc_2O_3-1 mol% M_2O_3–ZrO_2 ceramics, J. Am. Ceram. Soc. 95 (2012) 1965–1972.
[15] A. Spirin, V. Ivanov, A. Nikonov, A. Lipilin, S. Paranin, V. Khrustov, A. Spirina, Scandia – stabilized zirconia doped with yttria: synthesis, properties, and ageing behavior, Solid State Ion. 225 (2012) 448–452.
[16] V.V. Lakshmi, R. Bauri, Phase formation and ionic conductivity studies on ytterbia co-doped scandia stabilized zirconia ($0.9ZrO_2$–$0.09Sc_2O_3$–$0.01Yb_2O_3$) electrolyte for SOFCs, Solid State Sci. 13 (2011) 1520–1525.
[17] M.A. Borik, S.I. Bredikhin, A.V. Kulebyakin, I.E. Kuritsyna, E.E. Lomonova, F. O. Milovich, V.A. Myzina, V.V. Osiko, V.A. Panov, P.A. Ryabochkina, S. V. Seryakov, N.Yu. Tabachkova, Melt growth, structure and properties of $(ZrO_2)_{1-x}(Sc_2O_3)_x$ solid solution crystals ($x=0.035-0.11$), J. Cryst. Growth 443 (2016) 54–61.
[18] J. Fleig, J. Maier, The impedance of ceramics with highly resistive grain boundaries: validity and limits of the brick layer model, J. Eur. Ceram. Soc. 19 (1999) 693–696.
[19] H. Fujimori, M. Yashima, M. Kakihana, M. Yoshimura, β-cubic phase transition of scandia-doped zirconia solid solution: calorimetry, X-Ray diffraction, and raman scattering, J. Appl. Phys. 91 (2002) 6493–6498.
[20] H. Fujimori, M. Yashima, M. Kakihana, M. Yoshimura, Structural changes of scandia-doped zirconia solid solutions: rietveld analysis and raman scattering, J. Am. Ceram. Soc. 81 (1998) 2885–2893.
[21] M. Yashima, K. Ohtake, M. Kakihana, H. Arashi, M. Yoshimura, Determination of tetragonal–cubic phase boundary of $Zr_{1-X}RXO_{2-X/2}$ (R=Nd, Sm, Y, Er and Yb) by raman scattering, J. Phys. Chem. Solids 57 (1996) 17–24.
[22] Y. Hemberger, N. Wichtner, C. Berthold, K.G. Nickel, Quantification of yttria in stabilized zirconia by raman spectroscopy, Int. J. Appl. Ceram. Technol. 13 (2016) 116–124.
[23] M. Yashima, M. Kakihana, M. Yoshimura, Metastable-stable phase diagrams in the zirconia-containing systems utilized in solid-oxide fuel cell application, Solid State Ion. 86 (1996) 1131–1149.
[24] J.A. Krogstad, S. Krämer, D.M. Lipkin, C.A. Johnson, D.R. Mitchell, J.M. Cairney, C.G. Levi, Phase stability of t'- zirconia-based thermal barrier coatings: mechanistic insights, J. Am. Ceram. Soc. 94 (2011) s168–s177.
[25] B. Butz, Yttria-Doped Zirconia as Solid Electrolyte for Fuel-Cell Applications, (Doctoral dissertation), Karlsruher Inst. für Technologie, Diss., 2009.
[26] K. Yu, A.V. Voron'ko, A.A. Gorbachev, Sobol, raman scattering and the structure of cubic solid solutions based on zirconium and hafnium dioxides, Phys. Solid State 37 (1995) 1039–1052.